Applied Catalysis B: Environmental 164 (2015) 144–150

Contents lists available at ScienceDirect

Applied Catalysis B: Environmental

journal homepage: www.elsevier.com/locate/apcatb

MoP nanosheets supported on biomass-derived carbon flake: One-step facile preparation and application as a novel high-active electrocatalyst toward hydrogen evolution reaction

Wei Cui[a,b], Qian Liu[a], Zhicai Xing[a], Abdullah M. Asiri[c,d], Khalid A. Alamry[c,d], Xuping Sun[a,c,d,*]

[a] State Key Laboratory of Electroanalytical Chemistry, Changchun Institute of Applied Chemistry, Chinese Academy of Sciences, Changchun 130022, Jilin, China
[b] Graduate School of the Chinese Academy of Sciences, Beijing 100039, China
[c] Chemistry Department, Faculty of Science, King Abdulaziz University, Jeddah 21589, Saudi Arabia
[d] Center of Excellence for Advanced Materials Research, King Abdulaziz University, Jeddah 21589, Saudi Arabia

ARTICLE INFO

Article history:
Received 19 April 2014
Received in revised form 11 August 2014
Accepted 5 September 2014
Available online 16 September 2014

Keywords:
MoP nanosheets
Carbon flake
Biomass
Hydrogen evolution reaction electrocatalyst
Acidic and neutral electrolytes

ABSTRACT

Searching for Pt-free hydrogen evolution reaction (HER) electrocatalysts based on low-cost and earth-abundant materials is a crucial task for hydrogen-based energy industry. In this work, we demonstrate the one-step facile preparation of MoP nanosheets supported on carbon flake via a solid-state reaction with the use of $(NH_4)_6Mo_7O_{24}{\cdot}4H_2O$, $NaH_2PO_4{\cdot}2H_2O$ and a biomass, sodium alginate, as Mo, P and C sources, respectively. When used as a novel HER electrocatalyst, such composites are excellent in activity and durability in acidic electrolytes. Moreover, they are also active in neutral electrolytes.

1. Introduction

Hydrogen is an abundant, renewable and the cleanest fuel with zero-emission and represents one of the most promising energy sources [1]. Electrolysis of water is a cheap method for the production of highly pure hydrogen at the most economical price. As such, hydrogen production from water splitting has attracted growing attention [2]. An efficient hydrogen evolution reaction (HER) electrocatalyst is usually required to reduce the overpotential and consequently increase the electrochemical efficiency. Although the best current HER electrocatalysts are Pt-group metals, they suffer from scarcity and high cost limiting their wide use [2,3]. It is thus highly desirable to develop high-active HER catalysts based on low-cost, earth-abundant materials.

Recent years have witnessed the wide development of cheap Mo-based Pt-free HER electrocatalysts with high activity, including sulfide, carbide, nitride, boride and selenide, etc. [4–7]. MoP was proven to be a promising catalyst for a series of hydroprocessing reactions, such as hydrodeoxygenation (HDO), hydrodenitrogenation (HDN) and hydrodesulfurization (HDS) [8,9]. In addition, MoP was also predicated to have higher catalytic activity than MoC and MoN [10,11]. However, to the best of our knowledge, no attention has been paid to its utilization as a HER electrocatalyst before.

It is well established that electrocatalytic efficiency is mainly affected by morphology and electrical conductivity of catalysts [12]. Integration of catalysts with carbon leads to composites with increased dispersion of the active phases thus offering more active sites, improved mechanical strength and enhanced electrical conductivity [13,14]. In this study, we report on the facile preparation of MoP nanosheets supported on carbon flake (MoP/CF) via a solid-state reaction using $(NH_4)_6Mo_7O_{24}{\cdot}4H_2O$, $NaH_2PO_4{\cdot}2H_2O$ and a biomass, sodium alginate, as Mo, P and C sources, respectively. Such composites as a novel HER electrocatalyst show high activity and durability in acidic electrolytes. In addition, they can also operate in neutral medias.

* Corresponding author at: State Key Laboratory of Electroanalytical Chemistry, Changchun Institute of Applied Chemistry, Chinese Academy of Sciences, Changchun 130022, Jilin, China. Tel.: +86 0431 85262065; fax: +86 0431 85262065.
E-mail address: sunxp@ciac.ac.cn (X. Sun).

http://dx.doi.org/10.1016/j.apcatb.2014.09.016
0926-3373/

2. Experimental

2.1. Materials

Ammonium molybdate tetrahydrate ($(NH_4)_6Mo_7O_{24}{\cdot}4H_2O$) was purchased from Tianjin chemical Reagent Corp. (China). Sodium alginate ($(C_6H_7O_6Na)_n$) was purchased from Tianjin Guangfu Fine Chemical Research Institute (China). $NaH_2PO_4{\cdot}2H_2O$, KH_2PO_4 and $K_2HPO_4{\cdot}3H_2O$ were purchased from Beijing Chemical Corp. (China). H_2SO_4 was purchased from Aladdin Ltd. (Shanghai, China). Pt/C (20 wt% Pt on Vulcan XC-72R) and Nafion (5 wt%) were purchased from Sigma–Aldrich. All chemicals were used as received without further purification. The water used throughout all experiments was purified through a Millipore system.

2.2. Preparation of MoP/CF, bulk MoP and pure carbon flake (CF)

To prepare MoP/CF, 0.049 g $(NH_4)_6Mo_7O_{24}{\cdot}4H_2O$, 0.14 g $NaH_2PO_4{\cdot}2H_2O$ and 0.1 g $(C_6H_7O_6Na)_n$ were dissolved in water via ultrasonication for 30 min. The solution was dried at 85 °C and the resulting solid mixture was then calcined at 900 °C for 6 h with a rate of 10 °C min^{-1} in Ar atmosphere. After cooled to room temperature naturally, the solid products were washed with distilled water for several times to remove the residue of reactants, followed by dried at 80 °C. Bulk MoP was prepared via the same temperature program as MoP/CF, without introducing $(C_6H_7O_6Na)_n$. CF was prepared by pyrolysis of pure $(C_6H_7O_6Na)_n$ with the same temperature program under Ar flow.

2.3. Fabrication of the catalysts modified glassy carbon electrode (GCE)

To prepare the working electrode, 5 mg of the catalyst and 10 μL of 5 wt% Nafion solution were dispersed in 1 mL of water/ethanol (49:50, v/v) mixed solvent, followed by ultrasounded at least 30 min. Then 5 μL of the ink was dropped onto the glassy carbon electrode (loading: ~0.36 mg cm^{-2}).

2.4. Characterizations

Atomic force microscopy (AFM) characterization was performed on a MultiMode-V (Veeco Metrology, Inc.). Transmission electron microscopy (TEM) measurements were made on a Hitachi H-8100 electron microscope (Hitachi, Tokyo, Japan) with an accelerating voltage of 200 kV. X-ray diffraction (XRD) data were recorded on a RigakuD/MAX 2550 diffractometer with Cu Kα radiation (λ = 1.5418 Å). X-ray photoelectron spectroscopy (XPS) experiments were made on an ESCALABMK II X-ray photoelectron spectrometer using Mg as the exciting source. Gas chromatography (GC) measurements were carried out on GC-2014C (Shimadzu Co.) with thermal conductivity detector and nitrogen carrier gas.

2.5. Electrochemical measurements

Electrochemical measurements were performed with a CHI614D electrochemical analyzer (CH Instruments, Inc., Shanghai). A three-electrode cell was used, including a catalysts modified GCE as the working electrode, a saturated calomel electrode (SCE) as the reference electrode and a platinum wire as the counter electrode. For HER test in acidic environment, linear sweep voltammograms (LSVs) were collected with a scan rate of 2 mV s^{-1} in the range from 0 to −0.8 V vs. SCE in N_2 saturated aqueous solution of 0.5 M H_2SO_4. Cyclic voltammograms (CVs) were collected at a scan rate of 100 mV s^{-1} from −0.6 to −0.2 V vs. SCE for 3000 cycles. For HER test in neutral environment (pH = 7), a phosphate buffer solution (1 M) was used as the electrolyte. LSVs were collected in the range from −1.2 V to −0.4 V vs. SCE. Durability test was also carried out in the range from −1.0 to −0.6 V vs. SCE. Tafel plots are fit into the Tafel equation ($\eta = b\log(j) + a$, where b is the Tafel slope). Electrochemical impedance spectroscopy (EIS) measurements were carried out in the frequency range of 100 kHz–0.01 Hz.

In all measurements, SCE was used as the reference electrode, and all the potentials reported in our work were vs. the reversible hydrogen electrode (RHE). In 0.5 M H_2SO_4, E (RHE) = E (SCE) + 0.279 V. When pH = 7, E (RHE) = E (SCE) + 0.655 V.

The number of active sites (n) is examined using CVs in pH = 7 phosphate buffer at a scan rate of 100 mV s^{-1}. When the number of voltammetric charges (Q) is obtained after deduction of the blank value, n (mol) can be calculated with the following equation:

$$n = Q/2F$$

where F is Faraday constant (96,485 C mol^{-1}).

3. Results and discussion

Fig. 1a presents the XRD pattern of the as-prepared MoP/CF and bulk MoP. Same characteristic peaks are observed at 27.9, 32.2, 43.1, 57.5, 57.9, 64.9, 67.0, 67.9 and 74.3°, corresponding to the (0 0 1), (1 0 0), (1 0 1), (1 1 0), (0 0 2), (1 1 1), (2 0 0), (1 0 2) and (2 0 1) facets of MoP, respectively, (JCPDS No. 24-0771). The energy dispersive spectrum (EDS) reveals the presence of C, O, Mo and P elements in MoP/CF (Fig. 1b). The observation of C and O elements can be attributed to the formation of O heteroatoms incorporated carbon from carbonized sodium alginate [15]. Fig. 1c shows the low magnification TEM image of the composites, suggesting the formation of dark, thin, and flaky nanostructured stacks support on another flake. A more close view of such nanostructure (Fig. 1d) suggests that it consists of nanosheets with high radial–axial ratios. The high-resolution TEM (HRTEM) image taken from such nanosheet (Fig. 1e) reveals clear lattice fringes with an interplane distance of 0.28 nm corresponding to the (1 0 0) plane of MoP. In contrast, the HRTEM image (Fig. 1f) of the flake support shows that it is amorphous carbon in nature [16]. All these observations clearly confirm the formation of carbon flake (CF) supported MoP nanosheets. The thickness of one MoP nanosheet was measured to be around 1.6 nm (Fig. S1). It is worth while mentioning that the same preparation without the presence of sodium alginate only leads to bulk MoP (Fig. 1g), but the pyrolysis of pure sodium alginate only gives CFs (Fig. 1h) [17]. The thickness of CFs was measured by section analysis to be 2.26 nm (Fig. S2).

XPS analysis was performed to characterize the chemical states of MoP in the composites. Fig. 2a–c present the high-resolution Mo 3d, P 2p and C 1s XPS spectra. Peaks centered at binding energy of 228.2 and 232.1 eV in Mo 3d region (Mo $3d_{5/2}$) and 129.8 eV in P 2p region (P $2p_{3/2}$) are typical peaks for MoP [18–20]. Another peak at 131.5 eV in P 2p spectrum is assigned to C–P bond resulting from incorporation of P into carbon [21]. Three peaks are located at the binding energy of 283.5, 284.8 and 286.5 eV in deconvoluted C 1s spectrum, which can be assigned to the C–P, C–C and C–O bonds, respectively [21,22]. The weight ratio of Mo in MoP/CF was measured to be 9.85%, implying the weight ratio of MoP in MoP/CF is about 13.07%. The binding energy of Mo in the product is higher than metallic Mo^0 (227.6 eV) species, noting a partial positive charge, which results in a decrease in electron density of Mo 3d. Besides, the binding energy of P (129.8 eV) in MoP is lower than that of pure red phosphorus (130.1 eV), indicating a partial negative charge. Fig. S3a and S3b shows the Mo 3d and P 2p spectra of bulk MoP, respectively. Like MoP/CF, Mo peaks in bulk MoP locate in higher binding energy than metallic Mo^0 species and P peak locate in lower binding energy than pure red phosphorus. As

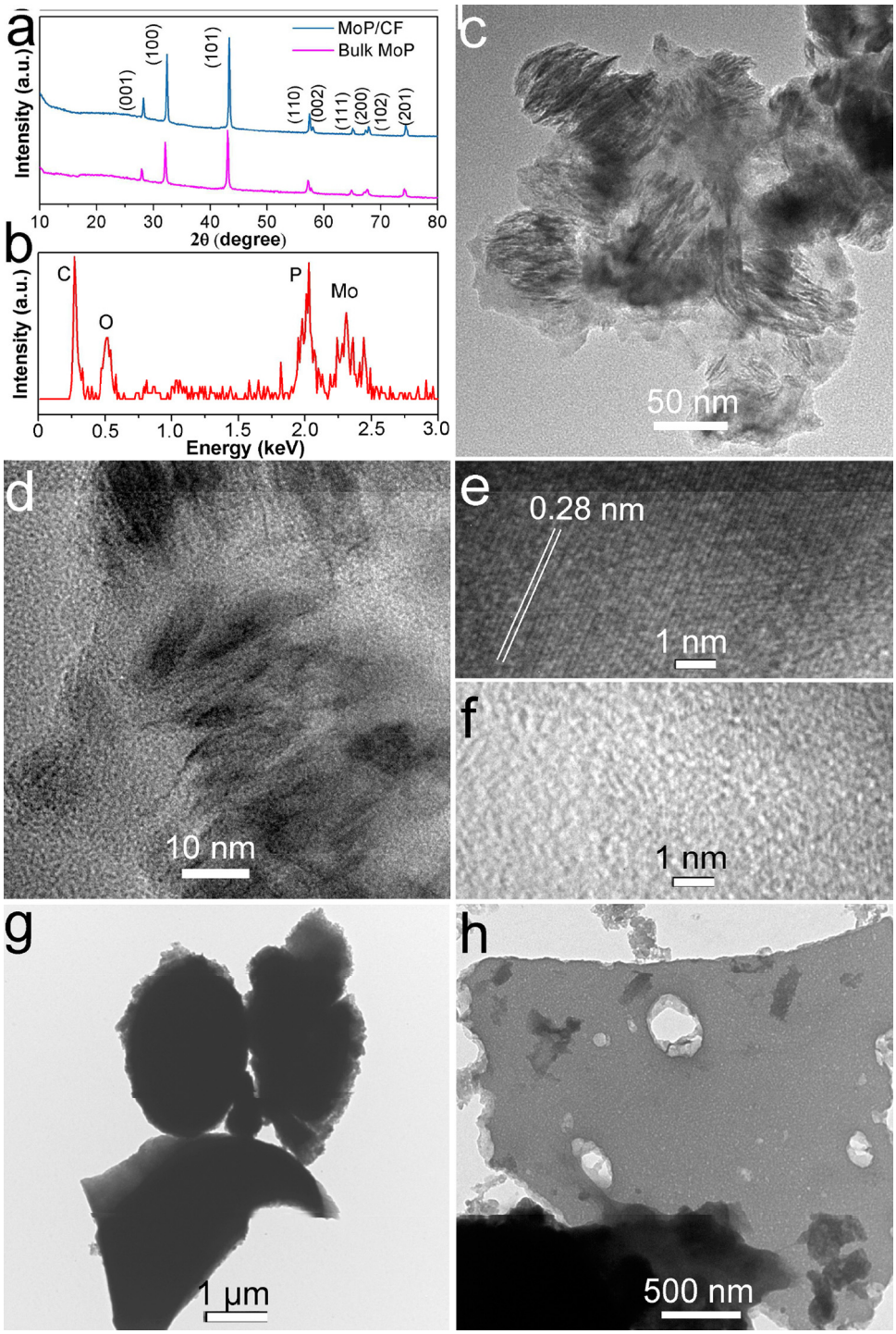

Fig. 1. (a) XRD patterns of MoP/CF and bulk MoP. (b) EDS, (c) low and (d) high magnification TEM images, and (e and f) HRTEM images of MoP/CF. TEM images of (g) bulk MoP and (h) CFs.

a consequence, a small transfer of electron density from Mo to the P occurs in MoP (bulk MoP and MoP/CF [23–25]. Besides, P 2p spectrum of bulk MoP and C 1s spectrum of CFs (Fig. S3c) exhibit less obvious peaks of C–P and C–O bonds, respectively.

Without any active process, the HER properties of all samples were directly examined. Electrocatalytic behaviors in acidic conditions (0.5 M H_2SO_4) were evaluated first using LSVs. Fig. 3a shows the polarization curves of MoP/CF, bulk MoP, CFs and Pt/C modified GCE. The CFs have little HER activity. Bulk MoP exhibits intrinsic catalytic activity toward HER with an onset potential of −0.20 V. In sharp contrast, MoP/CF shows greatly enhanced HER activity with a smaller onset overpotential (about 0.10 V), accompanied with large cathodic current densities. Only an overpotential (η) of less than 0.2 V is required to achieve the current density (j) of 10 mA cm^{-2} (when j = 50 mA cm^{-2}, η = 0.31 V). Commercial Pt/C as a reference shows the best HER activity with a near zero onset overpotential. Fig. 3b shows the corresponding Tafel plots. The Tafel slope of MoP/CF is calculated as 56.4 mV dec^{-1}, suggesting that the Heyrovsky mechanism is mainly responsible for the HER process. Bulk MoP shows a much larger tafel slope (79.2 mV dec^{-1}). Typically, the

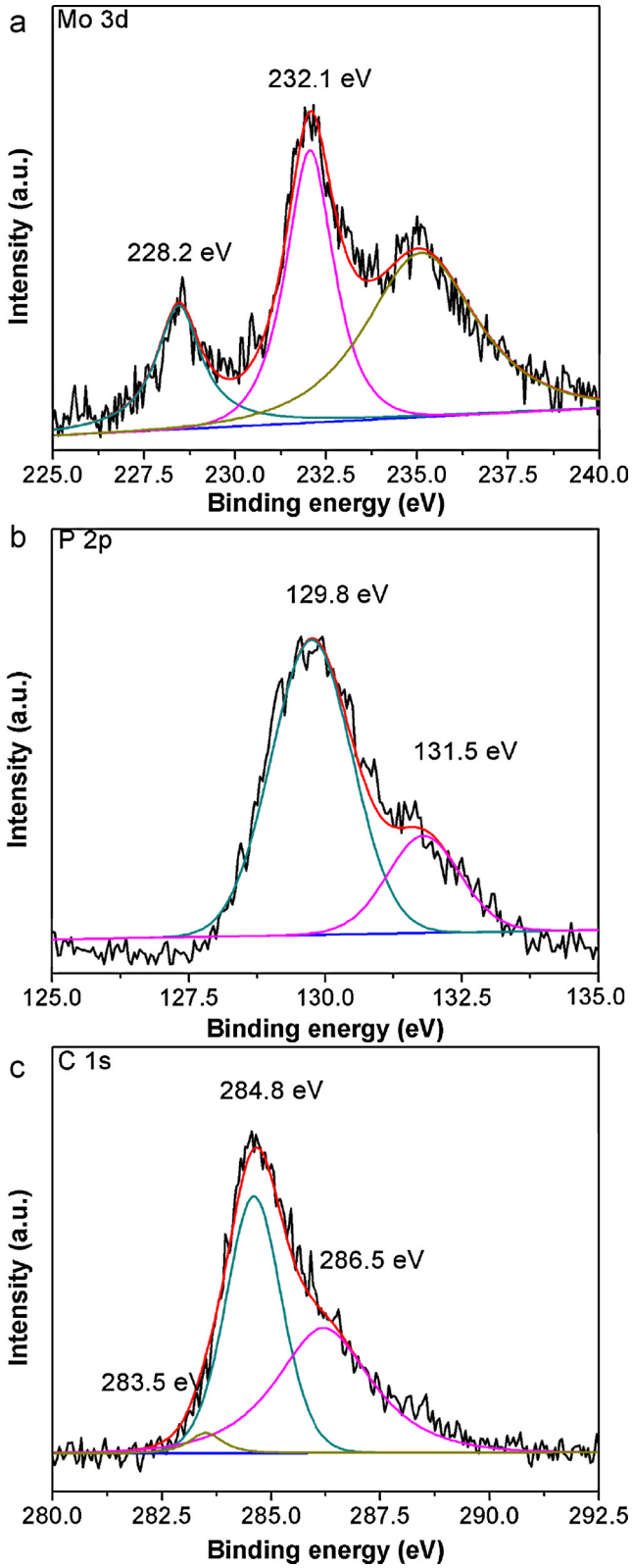

Fig. 2. XPS spectra of (a) Mo 3d, (b) P 2p and (c) C 1s regions of MoP/CF.

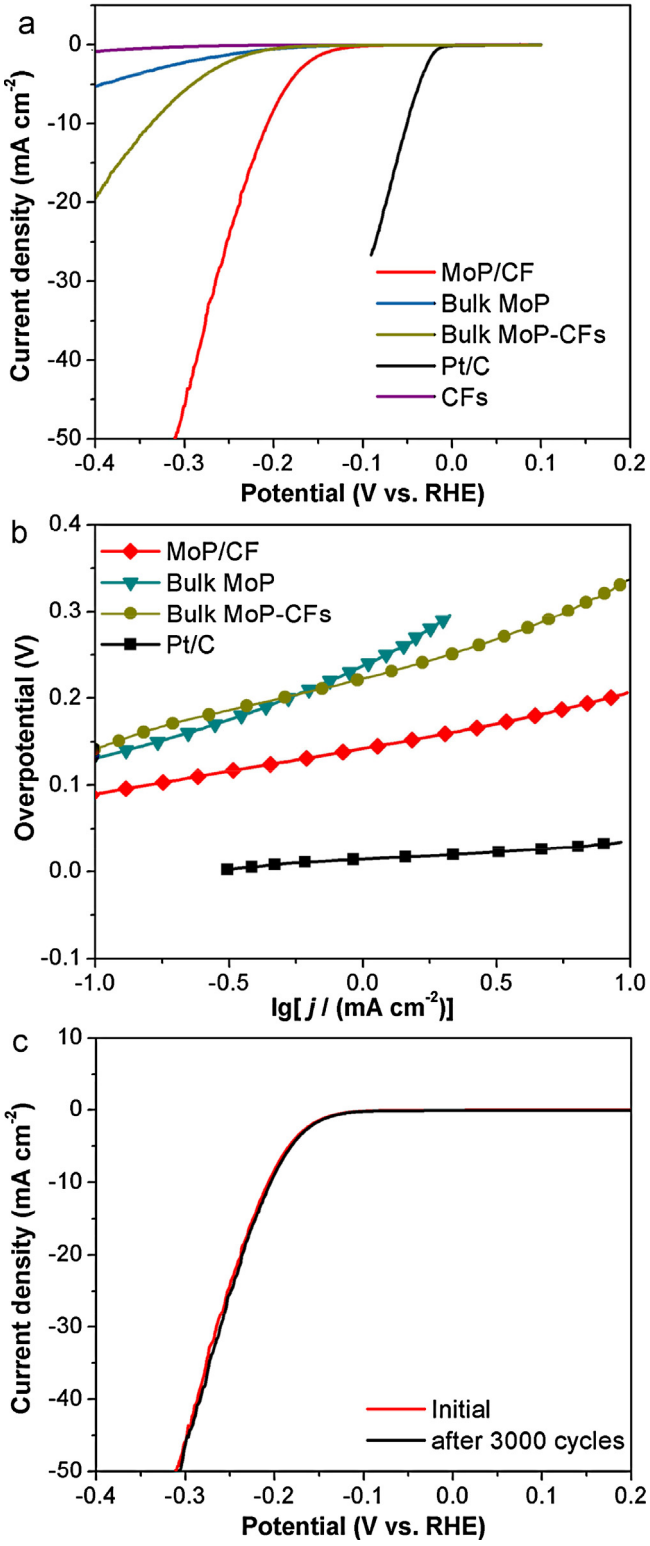

Fig. 3. (a) Polarization curves of MoP/CF, bulk MoP, CFs, Pt/C and bulk MoP-CFs modified GCE in 0.5 M H_2SO_4 at a scan rate of 2 mV s^{-1}. (b) Tafel plots of MoP/CF, bulk MoP, Pt/C and bulk MoP-CFs derived from their corresponding polarization curves. (c) Durability test for MoP/CF in 0.5 M H_2SO_4 for 3000 cycles.

Tafel slope of Pt/C is 30.0 mV dec^{-1}, suggesting the involvement of Tafel mechanism [26]. We also studied the catalytic behavior of the physical mixture of bulk MoP and CFs (bulk MoP-CFs) with the same weight ratio of MoP in MoP/CF. The bulk MoP-CFs exhibits enhanced activity compared to bulk MoP. However, MoP/CF still shows synergistically superior activity than bulk MoP-CFs, which can be ascribed to the stronger coupling between MoP and CF. In addition, bulk MoP-CFs shows a Tafel slope of 67.4 mV dec^{-1}, an intervenient value of Tafel slope between bulk MoP and MoP/CF. We further examined the corrosion stability of MoP/CF. As observed in Fig. 3c, there is negligible degradation between the first and the

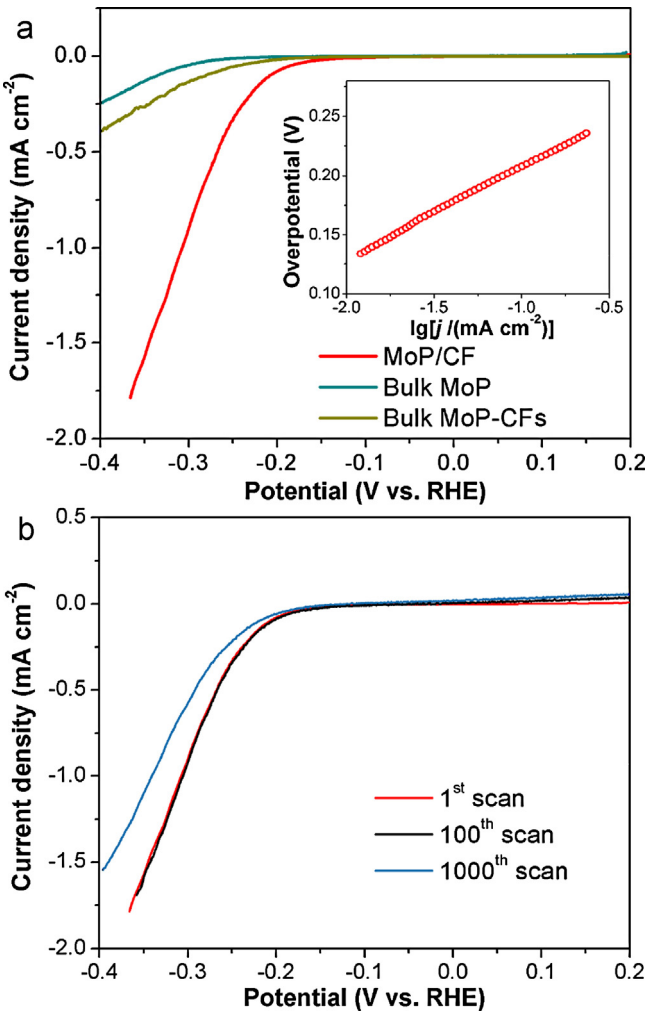

Fig. 4. (a) Polarization curves of MoP/CF, bulk MoP and bulk MoP-CFs modified GCE in 1 M phosphate buffer solution (pH 7). Inset: the linear region of the Tafel plot of MoP/CF. (b) Durability test for MoP/CF in 1 M phosphate buffer solution (pH = 7).

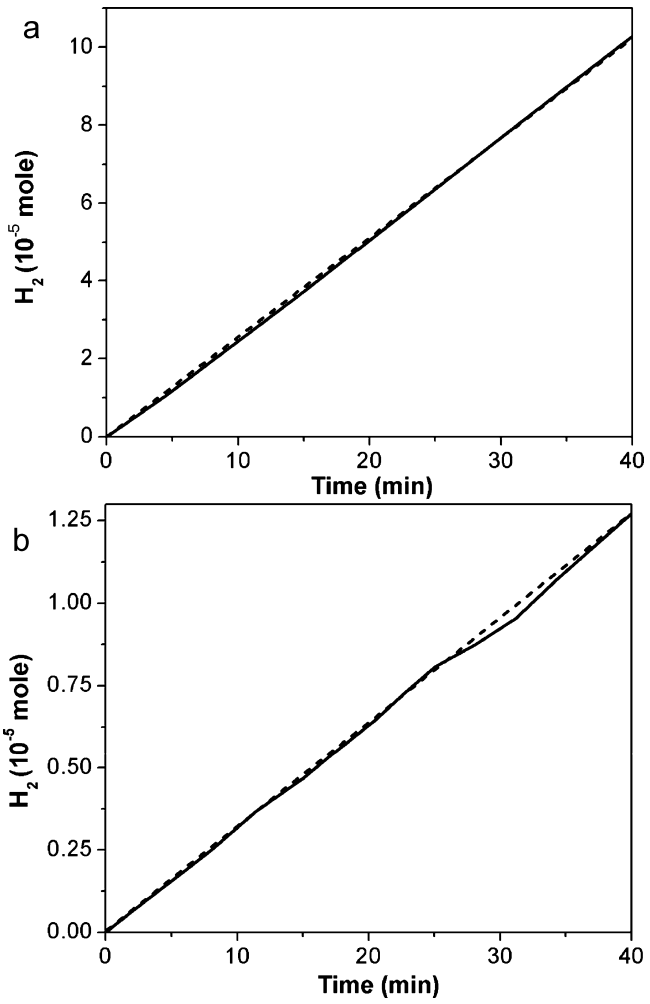

Fig. 5. The amount of calculated (dash) and experimentally measured (solid) hydrogen vs. time for MoP/CF at an overpotential of 250 mV for 40 min in (a) 0.5 M H_2SO_4 and (b) 1 M phosphate buffer solution (pH = 7).

3000th scan. All the results imply that MoP/CF shows excellent durability and thus is promising for practical applications. Table 1 shows HER activity parameters of several Mo compounds/carbon composites previously reported. MoP/CF shows high activity comparable with other catalysts with a small catalyst loading.

The strongly acidic conditions involved in proton exchange membrane technology need acid-stable HER catalysts [27,28]. However, electrohydrogenes are using microbial electrolysis cell as a promising approach for hydrogen production from organic matter typically operates at neutral pH suitable for microbial growth [29]. Accordingly, it is also highly desired to develop HER catalysts for use in neutral conditions to reduce environmental impact and increase biocompatibility [30]. The HER properties in neutral electrolyte for Mo compounds are rarely studied [7]. In present study, the HER properties of both MoP catalysts were also studied in 1 M phosphate buffer solution (pH = 7). Fig. 4a shows the polarization curves. MoP/CF still exhibits much better HER activity than bulk MoP, with a smaller onset overpotential (about 0.15 V). Compared with bulk MoP, significantly high current densities are achieved for MoP/CF at the same potentials. Similarly, bulk MoP-CFs exhibits higher activity than bulk MoP but lower activity than MoP/CF. Tafel slope for MoP/CF is calculated to be 77.8 mV dec^{-1} (Fig. 4a inset), which is a very decent value for a catalyst tested in neutral environment. The stability of MoP/CF in neutral conditions was then assessed. As shown in Fig. 4b, MoP/CF still retains the same catalytic performance after 100 cycles and obvious loss can be seen up to 1000 cycles. All these results clearly indicate that MoP/CF is also efficient toward HER in neutral conditions. Fig. S4 shows the TEM images of MoP/CF after cycling life tests in acidic and neutral conditions. No significant change in morphology is observed after cycling in acidic solution. In contrast, obvious aggregation occurs in neutral solution, which may adversely affect to electrochemical durability. The observations that the HER properties in neutral electrolyte are different with those in acidic electrolyte could be due to a higher solution resistance and less effective proton transport under neutral condition, but the exact reason is not completely understood at present time [7].

The generated gas was confirmed by GC analysis and measured quantitatively using a calibrated pressure sensor to monitor the pressure change in the cathode compartment of a H-type electrolytic cell. Potentiostatic cathodic electrolysis was carried out by maintaining catalyst-loaded glassy carbon plate (1 cm^2) at an overpotential of 250 mV for 40 min both in 0.5 M H_2SO_4 and 1 M phosphate buffer solution (pH = 7). The Faradic efficiency (FE) was calculated by comparing the amount of measured hydrogen with calculated hydrogen (assuming 100% FE), as shown in Fig. 5. Virtually 100% FE was obtained in both acidic and neutral conditions, suggesting the current density is directly related to hydrogen generation.

The EIS measurements show that MoP/CF has a much smaller semicircle of Nyquist plot than bulk MoP (Fig. 6a). It indicates that

Table 1
Comparison of HER parameters of several Mo compounds/carbon catalysts.

Catalysts	Loading (mg cm^{-2})	Electrolyte	j at η = 200 mV vs. RHE (mA cm^{-2})	Tafel slope (mV dec^{-1})	Ref.
MoP/CF	0.36	0.5 M H_2SO_4	10.1	56.4	This work
Mo_2C/CNT	2	0.1 M $HClO_4$	>10	55.2	[5]
Mo_2C/XC	2	0.1 M $HClO_4$	8.1	59.4	[5]
Mo_1Soy/RGO	—	0.1 M $HClO_4$	>12	62.7	[6]
$NiMoN_x$/C	0.25	0.1 M $HClO_4$	~4.1	35.9	[7]
MoN/C	0.25	0.1 M $HClO_4$	~0.3	54.5	[7]
MoS_2/RGO	1	0.5 M H_2SO_4	>25	41	[4]

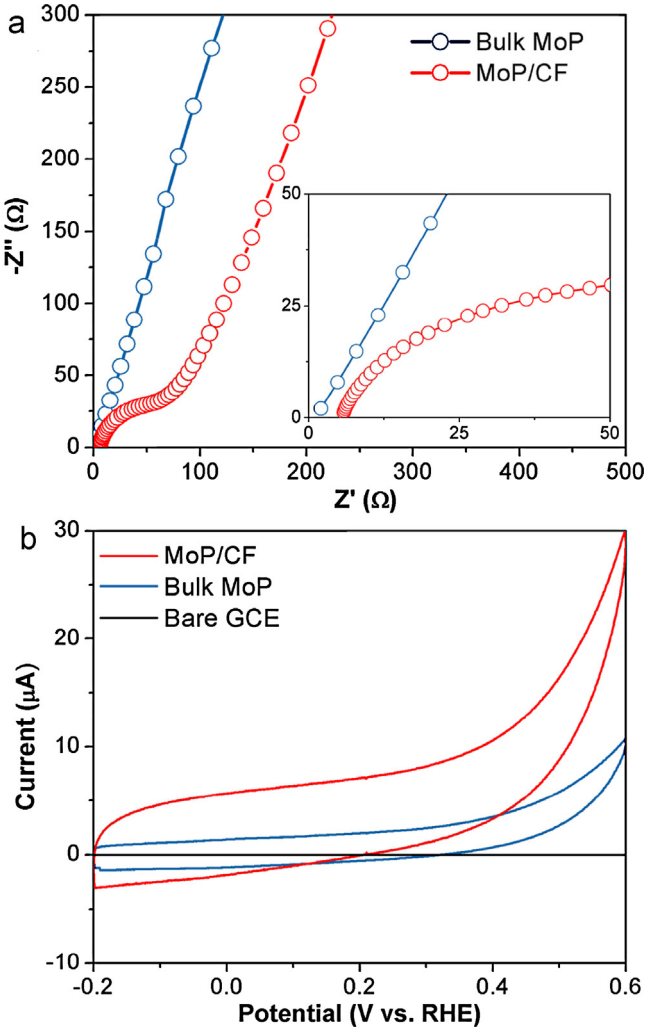

Fig. 6. (a) Nyquist plots of MoP/CF and bulk MoP (inset: a close view of high frequency region). (b) CVs of MoP/CF, bulk MoP and bare GCE recorded at pH = 7 with a scan rate of 100 mV s^{-1}.

MoP/CF has higher conductivity and thus better electron transfer ability than bulk MoP owing to the presence of conductive carbon support. The surface area of MoP/CF (22.90 m^2 g^{-1}) is quite larger than that of bulk MoP (0.97 m^2 g^{-1}). The surface area is also a critical factor for HER. Fig. S5 shows the N_2 adsorption–desorption isotherm of MoP/CF and bulk MoP. The surface area of MoP/CF (22.90 m^2 g^{-1}) is quite larger than that of bulk MoP (0.97 m^2 g^{-1}). In addition, the numbers of active sites for MoP/CF and bulk MoP were determined by CVs (Fig. 6b) to be 4.35×10^{-7} and 1.64×10^{-7} mol mg^{-1}, respectively, based on report method [31]. All these results can explain the superior HER performance of MoP/CF to bulk MoP.

It was reported that MoP shows good catalytic properties for the regeneration of the I_3^-/I^- redox couple as counter electrode (CE) material in dye-sensitized solar cells (DSCs) [32,33]. Basically, CE of DSCs performs two functions: collecting electrons and catalyzing the reduction of I_3^- to I^- ($I_3^- + 2e^- \rightarrow 3I^-$) [34]. In fact, the working electrode in HER process functions in a similar manner: transporting electrons and reducing H^+ to H_2 ($2H^+ + 2e^- \rightarrow H_2$) [35]. Previous DFT (density functional theory) calculations also demonstrate that MoP has certain Rh- and Pd-like properties [36]. So, it is not surprising to have found that MoP is capable of electrochemically catalyzing the reduction of H^+ to H_2. MoP possesses a tungsten carbide (WC)-type structure with each Mo atom being trigonal-prismatically surrounded by six P atoms [37]. It was reported that hydrogen-evolving metal complex catalyst incorporates proton relays from pendant acid–base groups proximate to the metal center where H_2 production occurs [38]. The active sites of hydrogenases also feature pendant bases positioned close to the metal centers [39]. The intrinsic HER activity for MoP in our present study could be explained as follows. In MoP, the Mo has a partial positive charge (δ^+) while the P has a partial negative charge (δ^-) due to transfer of electron density from Mo to P [40]. Like metal complex catalysts and hydrogenases, the surface of MoP nanosheet also features pendant base P (δ^-) close proximity to the metal center Mo (δ^+). Mo serves as the active center [41]. The Mo and P act as the hydride-acceptor and proton-acceptor center, respectively, facilitating the HER [42]. And at the same time, the presence of such P could also facilitate the formation of Mo-hydride for subsequent hydrogen evolution via electrochemical desorption [43]. Note that it should be much easier for P (δ^-) to form P–H ion pair with H^+ in acidic media than in neutral media. As a result, MoP is expected to have increased net positive charge and thus there is a stronger electrostatic repulsive interaction between MoP particles. That may explain why MoP agglomeration occurs in neutral condition not in acidic condition. Recently, Qiao group reported hetero-atom (N, P and S, etc.) doped carbon as efficient HER electrocatalysts [44]. Hetero-atom can reduce the ΔG_{H^*} values to promote the adsorption of initial H* with enhanced HER activity than pure carbon materials. Herein, C–P bonds in MoP/CF could be possible active sites toward the HER.

4. Conclusion

We have developed novel CF supported MoP nanosheets as a highly active HER electrocatalyst with excellent durability in acidic electrolytes. Such catalyst is also active in neutral media. The sodium alginate-derived CF not only prevents the MoP nanosheets from aggregation into bulk structure, but functions as a conductive support prompting electron transfer in the composites. Our present study provides us a general biomass-based strategy toward low-cost fabrication of nanostructured metal phosphide/C composites for HER and electrochemical energy storage applications [45].

Acknowledgements

This work was supported by the National Natural Science Foundation of China (No. 21175129) and the National Basic Research Program of China (No. 2011CB935800).

Appendix A. Supplementary data

Supplementary data associated with this article can be found, in the online version, at http://dx.doi.org/10.1016/j.apcatb.2014.09.016.

References

[1] G.W. Crabtree, M.S. Dresselhaus, M.V. Buchanan, Phys. Today 57 (2004) 39–45.
[2] M.G. Walter, E.L. Warren, J.R. McKone, S.W. Boettcher, Q.X. Mi, et al., Chem. Rev. 10 (2010) 6446–6473.
[3] D. Merki, X.L. Hu, Energy Environ. Sci. 4 (2011) 3878–3888.
[4] Y.G. Li, H.L. Wang, L.M. Xie, Y.Y. Liang, G.S. Hong, et al., J. Am. Chem. Soc. 133 (2011) 7296–7299.
[5] W.F. Chun, C.H. Wang, K. Sasaki, N. Marinkovic, W. Xu, et al., Energy Environ. Sci. 6 (2013) 943–951.
[6] W.F. Chen, S. Iyer, S. Iyer, K. Sasaki, C.H. Wang, et al., Energy Environ. Sci. 6 (2013) 1818–1826.
[7] W.F. Chen, K. Sasaki, C. Ma, A.I. Frenkel, N. Marinkovic, et al., Angew. Chen. Int. Ed. 51 (2012) 6131–6135.
[8] K.L. Li, R.J. Wang, J.X. Chen, Energy Fuels 25 (2011) 854–863.
[9] V.M.L. Whiffen, K.J. Smith, Top. Catal. 55 (2012) 981–990.
[10] P. Liu, J.A. Rodriguez, Catal. Lett. 91 (2003) 247–252.
[11] Z.W. Yao, Z.C. Lai, X.H. Zhang, F. Peng, H. Yu, et al., Mater. Res. Bull. 46 (2011) 1938–1941.
[12] L. Liao, J. Zhu, X.J. Bian, L.N. Zhu, M.D. Scanlon, et al., Adv. Funct. Mater. 23 (2013) 5326–5333.
[13] K.P. de Jong, Curr. Opin. Solid State Mater. Sci. 4 (1999) 55–62.
[14] Y.Y. Liang, Y.G. Li, H.L. Wang, H.J. Dai, J. Am. Chem. Soc. 135 (2013) 2013–2036.
[15] E. Raymundo-Piñero, F. Leroux, F. Béguin, Adv. Mater. 18 (2006) 1877–1882.
[16] L. Nistor, V. Ralchenko, I. Vlasov, A. Khomich, R. Khmelnitskii, et al., Phys. Stat. Sol. 186 (2001) 207–214.
[17] P. Atienzar, A. Primo, C. Lavorato, R. Molinari, H. García, Langmuir 29 (2013) 6141–6146.
[18] I.I. Abu, K.J. Smith, Catal. Today 125 (2007) 248–255.
[19] V.M.L. Whiffen, K.J. Smith, Energy Fuels 24 (2010) 4728–4737.
[20] I.I. Abu, K.J. Smith, J. Catal. 241 (2006) 356–366.
[21] M. Latorre-Sánchez, A. Primo, H. García, Angew. Chem. Int. Ed. 52 (2013) 11813–11816.
[22] T.I.T. Okpalugo, P. Papakonstantinou, H. Murphy, J. McLaughlin, N.M.D. Brown, Carbon 43 (2005) 153–161.
[23] X.H. Yan, J.Q. Sun, Y.W. Wang, J.F. Yang, J. Mol. Catal. A: Chem. 252 (2006) 17–22.
[24] K. Oshikawa, M. Nagai, S. Omi, J. Phys. Chem. B 182 (1999) 292–301.
[25] R. Wang, K.J. Smith, Appl. Catal. A: Gen. 361 (2009) 18–25.
[26] W.F. Chen, J.T. Muckerman, E. Fujita, Chem. Commun. 49 (2013) 8896–8909.
[27] G.A. Le, V. Artero, B. Jousselme, P.D. Tran, N. Guillet, et al., Science 326 (2009) 1384–1387.
[28] M. Hambourger, M. Gervaldo, D. Svedruzic, P.W. King, D. Gust, et al., J. Am. Chem. Soc. 130 (2008) 2015–2022.
[29] P.A. Selembo, M.D. Merrill, B.E. Logan, Int. J. Hydrogen Energy 35 (2010) 428–437.
[30] Y.J. Sun, C. Liu, D.C. Grauer, J. Yano, J.R. Long, et al., J. Am. Chem. Soc. 135 (2013) 17699–17702.
[31] D. Merki, S. Fierro, H. Vrubel, X.L. Hu, Chem. Sci. 2 (2011) 1262.
[32] M.X. Wu, J. Bai, Y.D. Wang, A.J. Wang, X. Lin, et al., J. Mater. Chem. 22 (2012) 11121–11127.
[33] M.S. Wu, J.F. Wu, Chem. Commun. 49 (2013) 10971–10973.
[34] G. Calogero, P. Calandra, A. Irrera, A. Sinopoli, I. Citro, et al., Energy Environ. Sci. 4 (2011) 1838–1844.
[35] D. Merki, H. Vrubel, L. Rovelli, S. Fierroand, X.L. Hu, Chem. Sci. 3 (2012) 2515–2525.
[36] Z.C. Feng, C.H. Liang, W.C. Wu, Z.L. Wu, R.A. van Santen, et al., J. Phys. Chem. B 107 (2003) 13698–13702.
[37] S.T. Oyama, P. Clark, X. Wang, T. Shido, Y. Iwasawa, et al., J. Phys. Chem. B 106 (2002) 1913–1920.
[38] A.D. Wilson, R.K. Shoemaker, A. Miedaner, J.T. Muckerman, D.L. Dubois, et al., Proc. Natl. Acad. Sci. U. S. A. 104 (2007) 6951–6956.
[39] Y. Nicolet, A.L. de Lacey, X. Vérnede, V.M. Fernandez, E.C. Hatchikian, et al., J. Am. Chem. Soc. 123 (2001) 1596–1601.
[40] S.T. Oyama, X. Wang, Y.K. Lee, K. Bando, F.G. Requejo, J. Catal. 210 (2002) 207–217.
[41] J. Kibsgaard, T.F. Jaramillo, F. Besenbacher, Nat. Chem. 6 (2014) 248–253.
[42] E.J. Popczun, J.R. McKone, C.G. Read, A.J. Biacchi, A.M. Wiltrout, et al., J. Am. Chem. Soc. 135 (2013) 9267–9270.
[43] W. Zhang, J.D. Hong, J.W. Zheng, Z.Y. Huang, J.R. Zhou, et al., J. Am. Chem. Soc. 133 (2011) 20680–20683.
[44] Y. Zheng, Y. Jiao, L.H. Li, T. Xing, Y. Chen, et al., ACS Nano. 8 (2014) 5290–5296.
[45] S. Carenco, D. Portehault, C. Boissière, N. Mézailles, C. Sanchez, Chem. Rev. 113 (2013) 7981–8065.